Modeling Permeability in Carbonate Rocks

Moustafa Dernaika[1,*], *Shehadeh* Masalmeh[1], *Bashar* Mansour[2], *Osama* Al-Jallad[2], and *Safouh* Koronfol[2]

[1]Abu Dhabi National Oil Company, EOR Department, 898 Abu Dhabi, UAE
[2]Halliburton, Ingrain, 114568 Abu Dhabi, UAE

Abstract. In carbonate reservoirs, permeability prediction is often difficult due to the influence of various geological variables that control fluid flow. Many attempts have been made to calculate permeability from porosity by using theoretical and empirical equations. The suggested permeability models have been questionable in carbonates due to inherent heterogeneity and complex pore systems. The main objective of this paper is to resolve the porosity-permeability relationships and evaluate existing models for predicting permeability in different carbonate rock types. Over 1000 core plugs were studied from 7 different carbonate reservoirs across the Middle East region. The plugs were carefully selected to represent main property variations in the cored intervals. The data set available included laboratory-measured helium porosity, gas permeability, thin-section photomicrographs and high-pressure mercury injection. Plug-scale X-ray CT imaging was acquired to ensure the samples were free of induced fractures and other anomalies that can affect the permeability measurement. Rock textures were analyzed in the thin-section photomicrographs and were classified based on their content as grainy, muddy and mixed. Special attention was given to the diagenesis effects mainly compaction, cementation and dissolution. The texture information was plotted in the porosity-permeability domain, and was found to produce three distinct porosity-permeability relationships. Each texture gave unique poro-perm trend, where the extent of the trend was controlled by diagenesis. Rock types were defined on each trend by detailed texture analysis and capillary pressure. Three different permeability equations (Kozney, Winland, Lucia) were evaluated to study their effectiveness in complex carbonate reservoirs. The texture-diagenesis based rock types provided more insight into the effects of geology on fluid flow and saturation. Available models may not fully describe permeability in heterogeneous rocks but they can improve our understanding of flow characteristics in various rock types.

1 Introduction

Core laboratory measurements can have a major impact on the reservoir modeling process [1]. Such measurements often yield unrepresentative results that raise questions about the effectiveness of the core data in the reservoir model and its calibration. This is partly related to the lack of understanding of reservoir heterogeneity as well as to the unrepresentative selection of plug samples. As a result, the data is often left unexplained, and there would be no link between the macroscopic measurements and fundamental microscopic properties or geological heterogeneities in the core [2]. Carbonates have complex and multimodal pore systems, therefore variation of permeability at single porosity can be very large (three to five orders of magnitude). This leads to poor porosity-permeability relationships [3] and imposes a challenge in classifying carbonates into rock types for proper permeability prediction. The porosity-permeability relationships can be resolved by additional information about the pore system, which is mainly related to the rock microstructure (texture) being grainy, muddy or mixed. The microstructure information can be obtained from thin-section photomicrographs. The microstructure (or texture) of the rock defines the pore geometrical properties regarding flow of fluids through the core and thus largely determine absolute permeability. The pore geometrical properties are mainly related to the medium of flow (texture), tortuosity and surface area. In this study, plug samples were selected to represent statistical distribution of porosity and textures in the reservoir cores. The porosity log was initially derived from dual energy core CT scanning [4] while the different textures were identified in the X-ray CT images [5]. The microstructure information of the plugs was confirmed from thin-section photomicrographs, and was plotted in the porosity-permeability domain. Samples with grainy microstructure gave high permeability while muddy samples showed lower permeability for the same porosity. The porosity and permeability data were fitted into unique trends based on the textural analysis. The different trends were mainly controlled by the different rock microstructures whereas the extent of the trend was due to different diagenesis processes (e.g. dissolution, cementation and compaction). Different permeability models were studied and evaluated for the established rock types.

2 Porosity-Permeability Relationships

In an earlier investigation [6], we studied 5 carbonate reservoir cores to understand the porosity-permeability relationships. Each cored interval ranged from 300 to over 500 feet, where some of the cores represented more than one formation. The cores were mainly limestone with highly varying porosity (~5% to 33%) and permeability (~0.01 mD to 5000 mD). Plug samples of 1.5” diameter were statistically selected to represent all the cored intervals. Two more reservoir cores were later evaluated, and all the 7 reservoir core (Poro-Perm) data are shown in

* Corresponding author: mdernaika@adnoc.ae

figure 1. The data present the conventionally-measured helium porosity and gas permeability on the selected plugs. The porosity and permeability data for each plug were associated with the sample texture that was identified from the corresponding thin-section photomicrograph. Figure 1 shows three distinct porosity-permeability trends from the analysed cores in all the 7 reservoirs. The textures of the samples were classified as grainy, mixed and muddy [7]. All the textures revealed large porosity ranges, which was the result of different degrees of leaching, cementation and compaction (*i.e.* diagenesis). The different textures had clear effects on the porosity-permeability relationships. The analysed samples and the porosity-permeability relationships are believed to be representative to the reservoir properties. This was possible by applying statistical sample selection based on high-resolution dual energy CT imaging of the entire cores [4,5,9]. The plugs were also imaged by X-ray CT to ensure the samples were free of induced fractures and other anomalies that may affect the permeability data. Without the plug-scale CT image it would not be possible to ensure representative plug measurements and thus conclusive poro-perm trends. More details on the importance of the plug CT can be found in [5]. The plug CT images were also used to select representative thin-sections and MICP trims from the mother plugs. This is a crucial requirement in heterogeneous reservoirs, where heterogeneity can have dramatic effects at the centimeter scale [10]. In each of the 7 reservoirs, it was possible to establish relationships between porosity and permeability in accordance to textural variation. The grainy, mixed and muddy textures seem to be the main controlling parameters in this relationship. We can see distinct porosity-permeability trends in relation to the three identified textures. It is important to note that there was no evidence of any kind of poro-perm data cloud in any of the analysed cores [6]. All the poro-perm characteristics were classified and described based on the rock textures (and diagenesis). Although the rock microstructure appears to be the main control of flow we should also notice the effects of the porosity type. For instance, a muddy carbonate may have 'touching vug' porosity with a very high permeability.

3 Texture-Based Rock Typing

In this research, we studied the rock types of the samples within each texture trend. The rock types (along each poro-perm trend) were identified based on the link between the sample's detailed Dunham texture [8], diagenesis and capillary pressure. Figure 2 shows examples from the effects of texture on capillary pressure (Pc) and pore-throat size distribution (PTSD) curves. The texture effect is shown for high porosity (around 25%) and low porosity (around 10%) samples (different diagenesis: here cementation). There is almost one order of magnitude (permeability) difference between the different textures at the same porosity. The grainy samples are characterised by larger pore throat sizes, lower entry pressure and higher permeability.

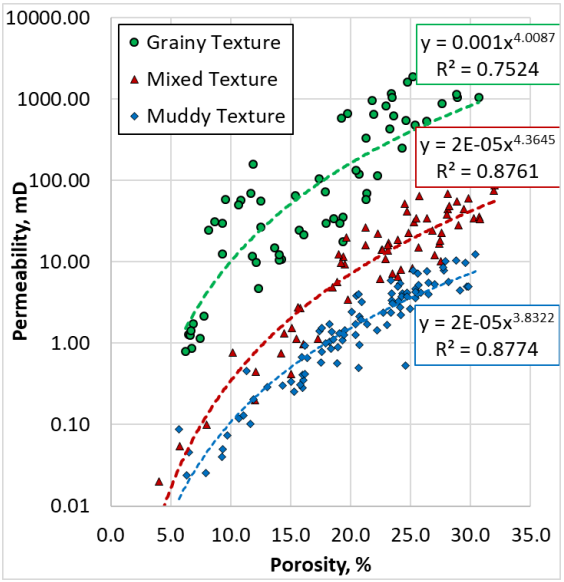

Fig. 1. Texture-Diagenesis based Poro-Perm trends in the 7 carbonate reservoirs in the Middle East region. Best fit along with correlation are given for each texture by power regression.

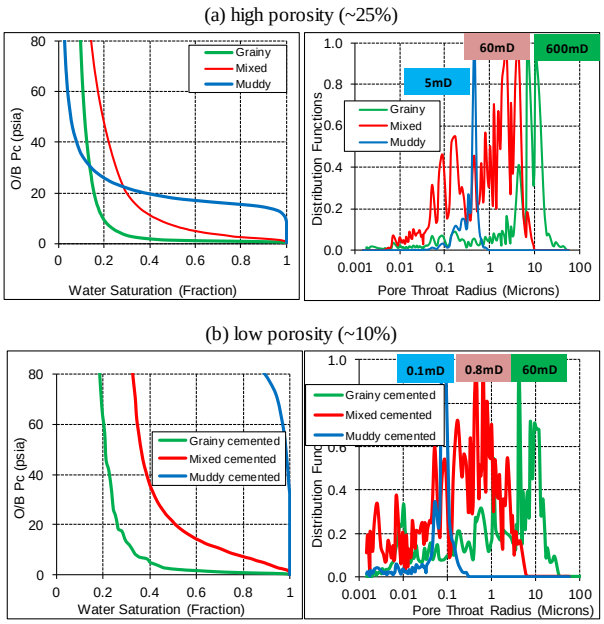

Fig. 2. Effect of texture on Pc and PTSD (a) at high porosity and (b) at low porosity

Initial water saturation (Swi) may not always be linked to permeability or texture in carbonates [12]. It is normally dependent on the Pc level as well as the percentage of the smallest pores in the rock beyond the applied Pc [11]. In figure 2a, for instance, the high-porosity muddy sample has lower Swi value (at high Pc) compared to the grainy and mixed texture samples. This is due to the fact that the mixed and grainy samples have more pore-throat fractions below 0.1micron as can be seen in the corresponding PTSD plot. Figure 3 shows the effect of porosity (mainly diagenesis) on the Pc and PTSD curves for each texture. It is seen that there is a good correlation between porosity and Swi within each texture: higher porosity within a single texture yields lower Swi. These plots demonstrate the influence of texture and diagenesis on petrophysical properties, hence confirming the importance of texture as

a fundamental tool for rock typing. Furthermore, this analysis emphasizes the need of rock typing within single textures.

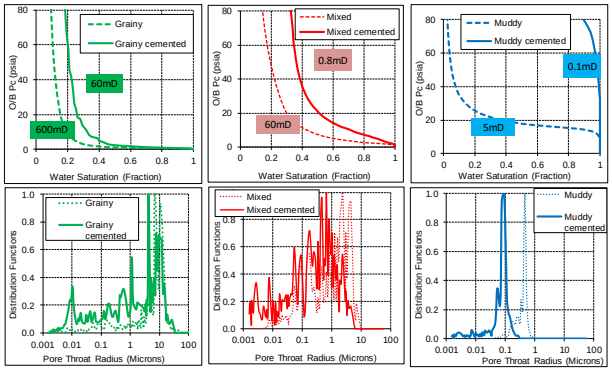

Fig. 3. Effect of porosity (diagenesis) on the Pc and PTSD curves for each texture

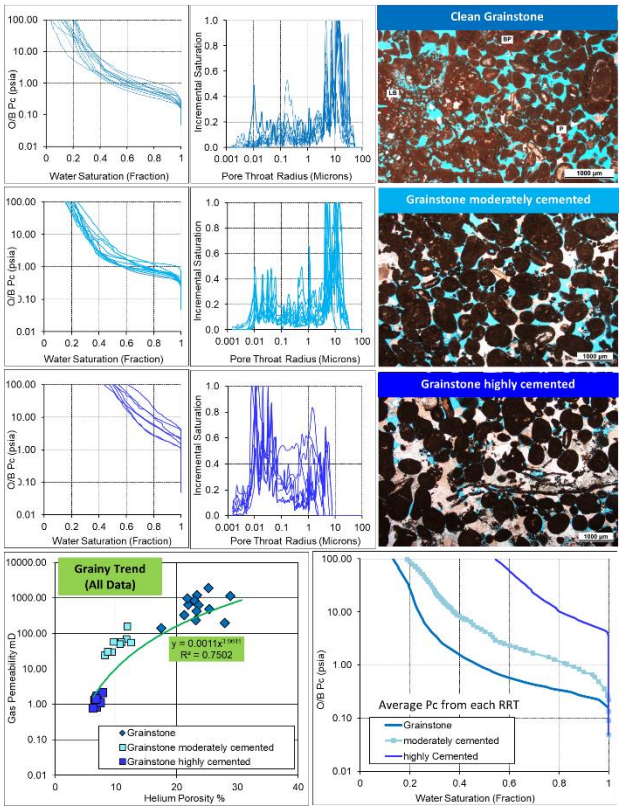

Fig. 4. Grainy Texture: 3 grainstone rock types. Samples from each RRT are presented with Pc/PTSD curves and a representative TS photomicrograph with Dunham classification. The poro-perm data are plotted with the main grainy trend from figure 1. Average Pc curves from all RRT's are plotted together.

4 The Rock Types

The rock types were established along the main texture (poro-perm) trends. They were identified over each texture based on Dunham classification and different diagenesis processes. The different geologically-defined rock types were correlated reasonably well with the poro-perm data and the MICP-derived Pc & PTSD curves. The mercury-derived Pc curves were converted to oil-water fluid system using interfacial tension of 32 mN/m. Figure 4 to figure 9 depict the main rock type characteristics found in the 7 carbonate reservoirs under study. Each figure gives all the rock types mainly within single texture classification along with their poro-perm data and mercury-derived Pc & PTSD. A representative thin-section photomicrograph is also depicted from each rock type. The main Dunham texture character of each rock type is indicated on the corresponding thin-section photomicrograph and in the legend of the poro-perm plot. The Pc curves are plotted in a semi-log format to show the capillarity behaviour more clearly. Within each rock type, all samples show consistent MICP and thin-section information with the poro-perm characteristics. A total of 25 rock types have been observed in these reservoirs. Some of the different textures may show similar drainage capillary behaviour but they can still be identified as different rock types based on the poro-perm data and other geological attributes. These rock types honour geological and static rock properties that should be further validated against dynamic data (*e.g.* imbibition capillary pressure and relative permeability) for ultimate reservoir modelling studies [12]. In this rock typing work, we indicated all the geological textures that we encountered in the studied reservoirs. Some of these textures may not have significant effects on the petrophysical properties and hence some of the identified rock types may be grouped into single RRT for practical reasons.

Grainy Texture: Grainstone RRT's

Figure 4 shows the grainy limestone rock types from the grainstone texture. There are 3 grainstone rock types with different degrees of cementation. The poro-perm data are plotted with the main grainy trend and show higher values than the average trend. The presence of cement largely affected the poro-perm characteristics and the corresponding Pc & PTSD curves. It is seen that the percentage of microporosity increases with cementation. The microporosity in these rock types is coming from micritization in the grains.

Grainy Texture: Rudstone RRT's

In figure 5, five rock types were identified, mainly from the Rudstone texture. The rock types show very heterogeneous PTSD curves due to large variations in grain sizes and pore sizes with different diagenetic footprints such as leaching and cementation. The best quality rock is the rudstone-to-boundstone texture while the poorest quality rock is the cemented rudstone. Two rock types were seen from the rud/bound-to-floatstone with higher percentage of floatstone in the rud/bound to floatstone2 as labelled in the corresponding legend in the figure. The higher micrite content is reflected in the PTSD curves. One more rock type was seen in this group, which is the rud-to-grainstone texture with intraparticle porosity. The rud-to-boundstone RRT show a main PTSD peak at around 100microns (~1000mD). The cemented rudstone rock type gives wide PTSD, while the rest of the rock types show bimodal PTSD.

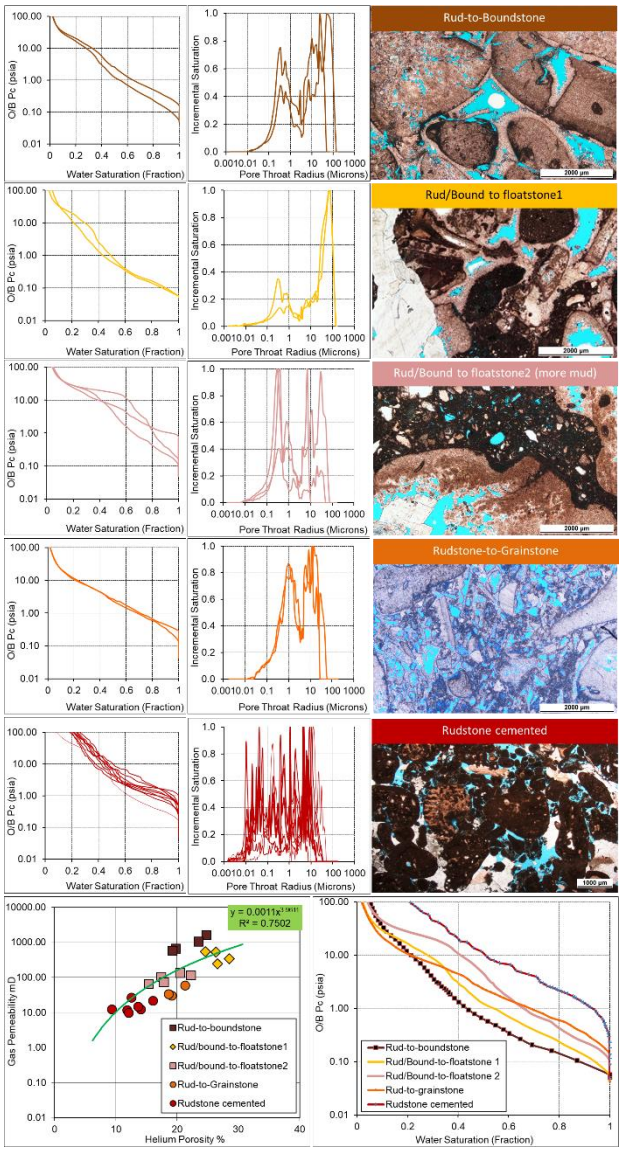

Fig. 5. Grainy Texture: 5 rudstone rock types.

Grainy Texture: Dolostone RRT's

Figure 6 shows 4 dolomitic RRT's with different degrees of leaching and compaction. The poro-perm data are seen lower than the average grainy trend. The rock types show narrow and uniform PTSD curves.

Mixed Texture: Packstone RRT's

Figure 7 shows the mixed limestone rock types from the packstone texture. There are 5 packstone rock types with different degrees of leaching, compaction and cementation. The poro-perm data are plotted with the main mixed trend. The presence of cement and compaction largely affected the poro-perm characteristics and the corresponding Pc & PTSD curves. Samples with less compaction/cementation (i.e. > 1mD) show heterogeneous PTSD.

Mixed Texture: Floatstone RRT's

In figure 8, three rock types were identified, mainly from the Floatstone texture. The main difference in these rock types is related to detailed textural facies with floatstone-to-boundstone being the best quality with highest permeability range and lowest Pc entry pressure. The lowest quality rock type is the bioturbated floatstone-to-packstone texture. The samples show the main PTSD peak less than 1micron. The tendency towards larger pore throats is caused due to leaching and presence of boundstone texture.

Muddy Texture: Wackstone/Mudstone RRT's

Figure 9 depicts 5 rock types from the wackstone/mudstone textures. The poro-perm data and Pc curves are largely influenced by cementation, recrystallization and compaction. All the samples have permeability less than 10mD, Pc entry pressure above 10psi (oil-water) and pore-throat radius below 1micron.

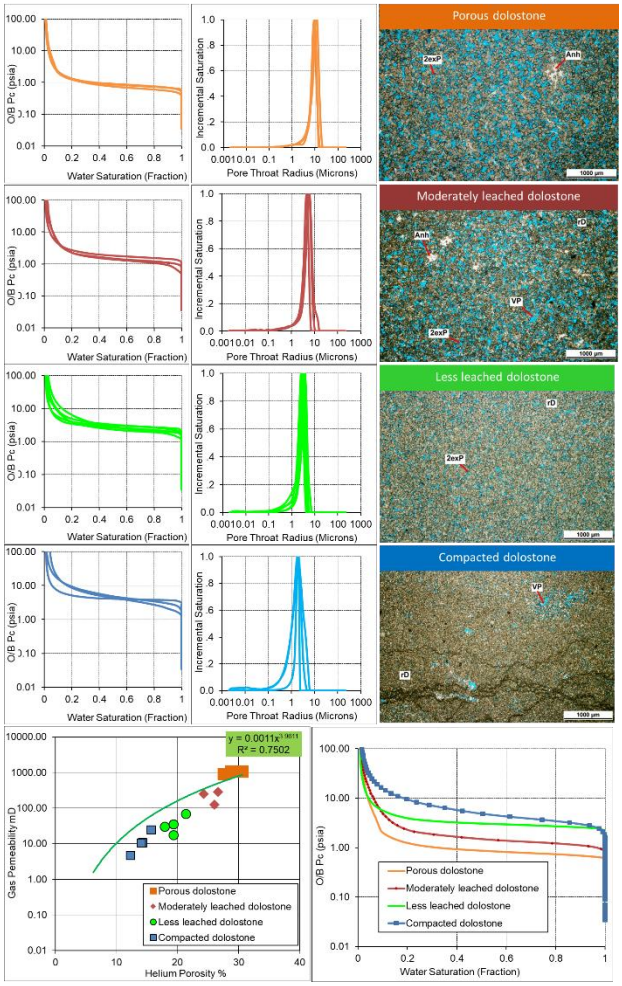

Fig. 6. Grainy Texture: 4 dolostone rock types.

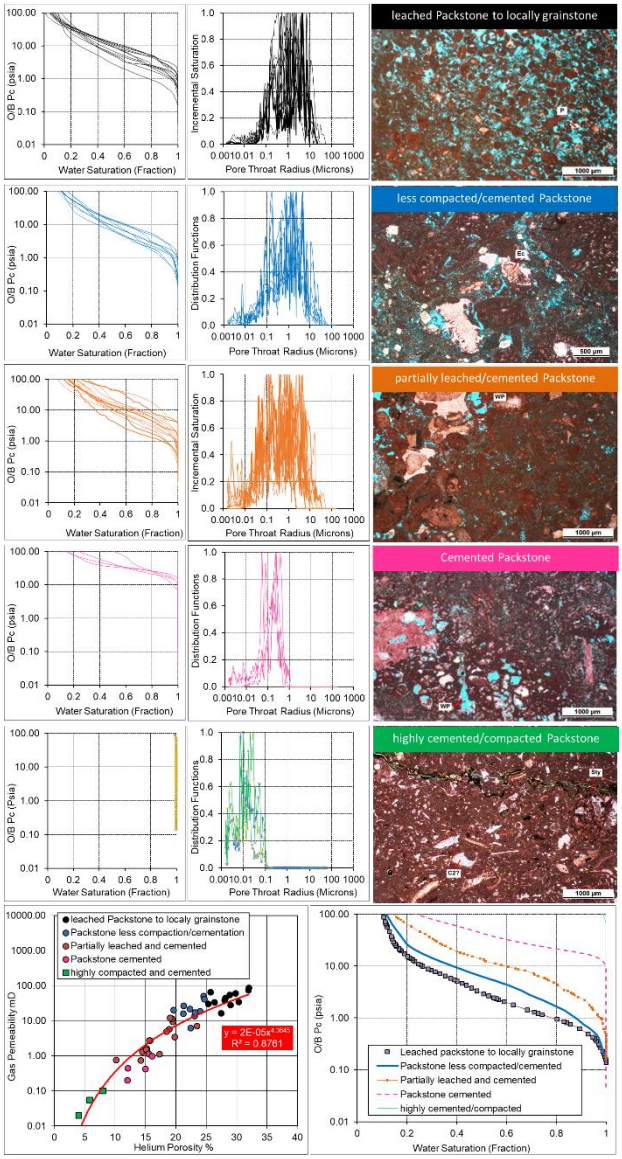

Fig. 7. Mixed Texture: 5 packstone rock types.

5 Permeability Estimation

Permeability estimation is an important step in reservoir characterisation for effective modeling of water-flood performance and subsequent Enhanced Oil Recovery (EOR) processes. The ultimate goal is to obtain permeability description as a function of reservoir space. This would require accurate determination of permeability versus depth in all logged wells in a field. This is normally achieved by the use of cross-plots of core permeability versus core porosity from log-derived porosity in uncored wells. The main aim of this research is to study the dependence of permeability on porosity and other geological attributes to provide guidelines for the establishment of accurate porosity-permeability cross-plots.

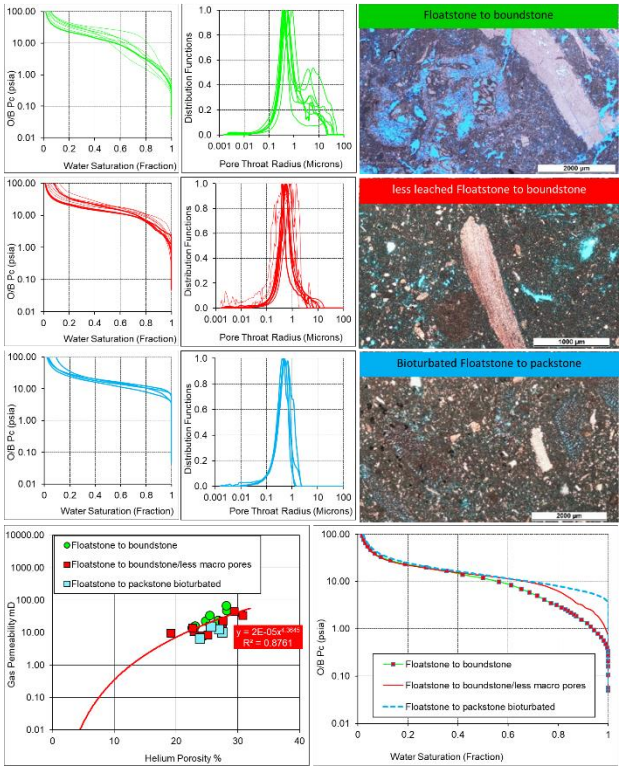

Fig. 8. Mixed Texture: 3 floatstone rock types.

5.1 Kozeny-Carmen Equation

Amaefule [13] proposed a permeability (k) model for identifying hydraulic units within mapable geological facies. The model is based on a modified Kozeny – Carmen equation and the concept of mean hydraulic radius. They derived equation (1), which indicates that for any hydraulic unit, a log-log plot of RQI versus Φz should yield a straight line with a unit slope,

$$RQI = \Phi z.FZI \qquad (1)$$

Where,

RQI is the Reservoir Quality Index (µm), $0.0314\sqrt{(k/\Phi)}$.

Φz is the Normalized Porosity Index (NPI), $\Phi/(1-\Phi)$.

FZI is the Flow Zone Indicator (µm); a unique parameter for each hydraulic unit, and is determined from the intercept of the unit slope line with Φz = 1.

Equation (1) is a reduced form of the modified Kozeny-Carmen equation below,

$$0.0314\sqrt{(k/\Phi)}=[\Phi/(1-\Phi)][1/(\sqrt{(F_s)}\ \tau.S_{gv}\ )] \qquad (2)$$

Where,

F_s stands for a shape factor (2 is for circular cylinder)

τ is the Tortuosity of the porous medium

S_{gv} is the surface area per unit grain volume

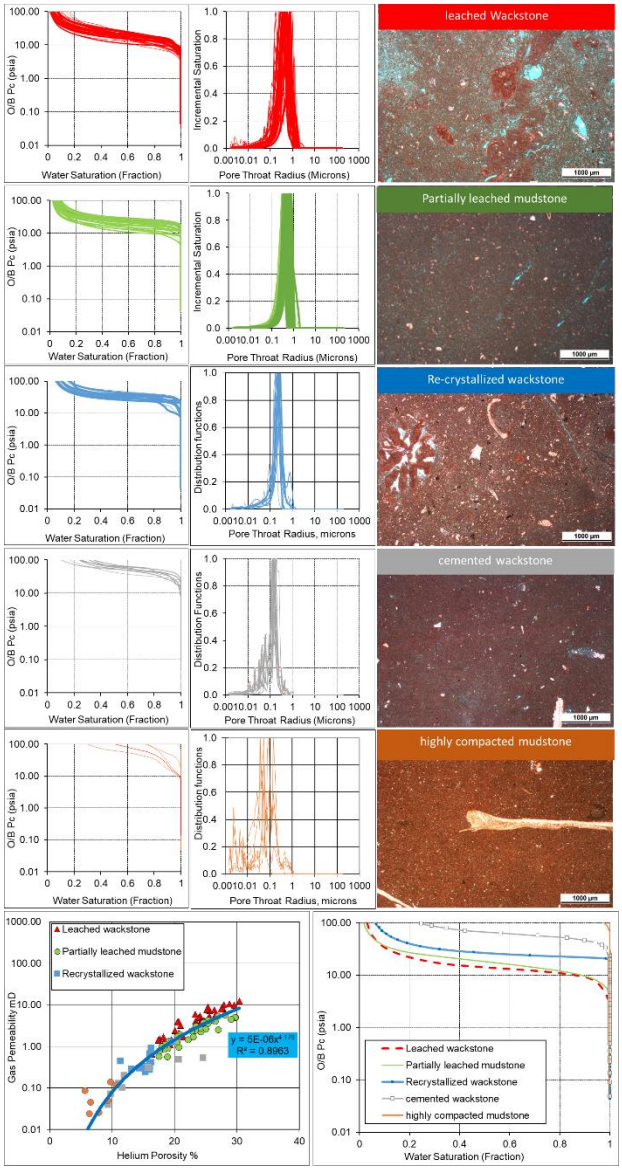

Fig. 9. Muddy Texture: 5 wackstone/mudstone rock types.

It is clear (from equations (1) and (2)) that FZI is related to the geological properties of the porous medium, being inversely proportional to the pore (throat) attributes. Therefore, samples with similar FZI value would constitute single hydraulic unit that is mainly defined by texture, poro-perm and capillary pressure.

Equation (3) is a developed relationship between permeability and FZI, derived from the generalized form of the Kozeny-Carmen relationship [13],

$$k=1014\,(FZI)^2\,[\Phi^3/(1-\Phi)^2] \qquad (3)$$

This permeability model has a theoretical basis with only one parameter, FZI, which offers a significant advantage over other methods for estimating permeability in un-cored wells [14]. Hence, it would be an excellent opportunity to use the well-established rock type data in the earlier section to examine the effectiveness of equation (3) in carbonate reservoirs. We should bear in mind that the theoretical equation is not expected to precisely model the measured poro-perm data because the derivation of the equation was made with certain assumptions that may not necessarily hold for natural porous media; the primary assumption is that the rock is composed of a bundle of capillary tubes [14,15].

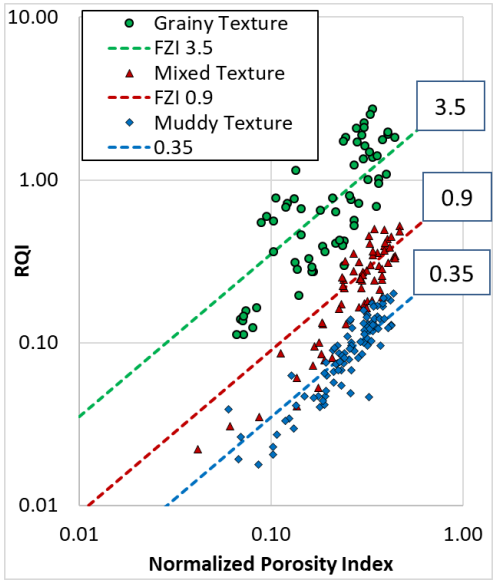

Fig. 10. RQI versus NPI for all the poro-perm data (from figure 1) plotted using equation 1. Grainy samples show an average FZI value of 3.5, Mixed 0.9 and Muddy 0.35.

Figure 10 plots the poro-perm data from figure 1 in the domain of RQI and NPI using equation (1). The grainy texture samples gave an average FZI of 3.5 while the mixed and muddy textures give FZI of 0.9 and 0.35, respectively. From equation (2), FZI is inversely proportional to pore shape, tortuosity and surface area. This means FZI is expected to be higher for porous media characterised by smaller surface area like the grainy texture, which is indeed consistent with the behaviour in figure 10. The pore shape factor and tortuosity may vary between textures and it would be more difficult to conclude about their effects on FZI. Actually, these pore throat attributes may vary within the same texture due to complex diagenesis processes, and this may explain the variation we already see in permeability within the same texture and porosity. Nevertheless, the strong trend we see between FZI and texture indicates the strong control of surface area on fluid flow in these carbonates. Figure 11 is rather a good representation of the FZI trends in the porosity-permeability domain by the use of equation (3). Figure 12 depicts the different grainy RRT's in the poro-perm plot. The data can be fitted with 3 different FZI values. The clean and partially cemented grainstone with Rud-to-Boundstone RRT's show similar FZI value of 6.5. The porous/leached dolomite with the Rud/Bound-to-floatstone RRT's have FZI 3.5. Less leached/compacted dolomite, highly cemented grainstone, rud-to-grainstone and cemented rudstone FZI value is 2. This clearly shows that FZI is not unique per RRT for the grainy texture samples. This statement is rather emphasized in figure 13, where the samples with similar FZI values are plotted together. Large variations are clearly seen in the Pc curves and pore structure (from thin-section photomicrographs)

within samples of the same FZI (even within similar porosity range). This means FZI cannot be considered as a good parameter to characterize hydraulic units, which are normally defined by texture, porosity-permeability characteristics and capillary pressure.

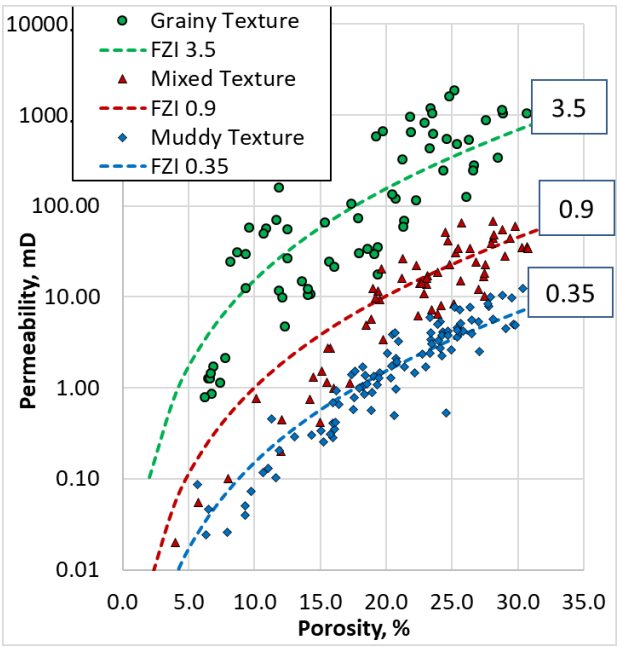

Fig. 11. Permeability versus porosity for all the poro-perm data (from figure 1) with FZI trends plotted from equation (3).

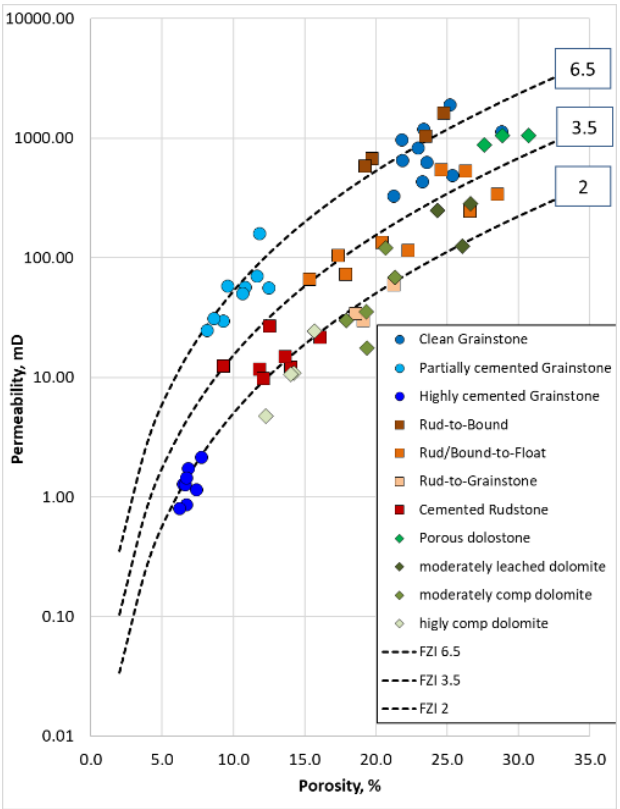

Fig. 12. Highlighted grainy RRT's with 3 different FZI values. Clean and partially cemented grainstone with Rud-to-Boundstone gave FZI 6.5. Porous/leached dolomite with Rud/Bound-to-floatstone FZI 3.5. Less leached/compacted dolomite, highly cemented grainstone, rud-to-grainstone and cemented rudstone FZI 2. FZI is not unique per RRT.

Figure 14 shows the mixed-texture RRT's with 2 different FZI values. The leached texture RRT's (i.e. packstone-to-grainstone, floatstone-to-boundstone and packstone) give FZI of 1 with porosity higher than 20%. The less leached textures give FZI 0.55 with the same porosity range. However, the cemented/compacted textures also give FZI 0.55 with porosity less than 20%. Figure 15(a) shows that the leached textures have similar RRT characteristics with similar FZI of 1. The less leached textures of similar porosity range (figure 15(b)) also show similar RRT characteristics and FZI of 0.55. The cemented/compacted packstone samples in figure 15(c) do not show the same consistency between FZI and the Pc curves.

(a) Grainy samples with similar FZI=6.5

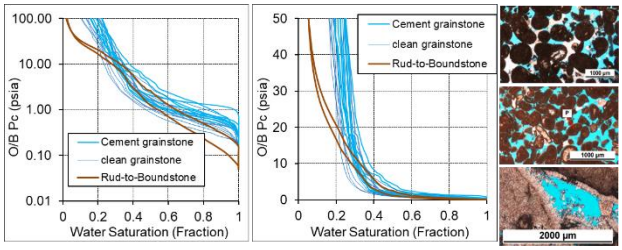

(b) Grainy samples with similar FZI=3.5

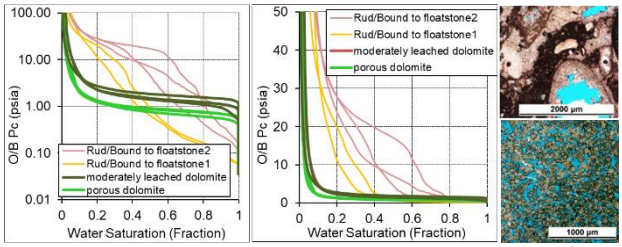

(c) Grainy samples with similar FZI=2

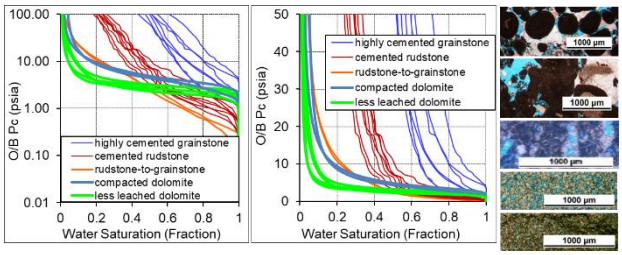

Fig. 13. Grainy RRT samples grouped by FZI. Samples with same FZI may not necessarily be of same RRT or demonstrate similar hydraulic flow unit.

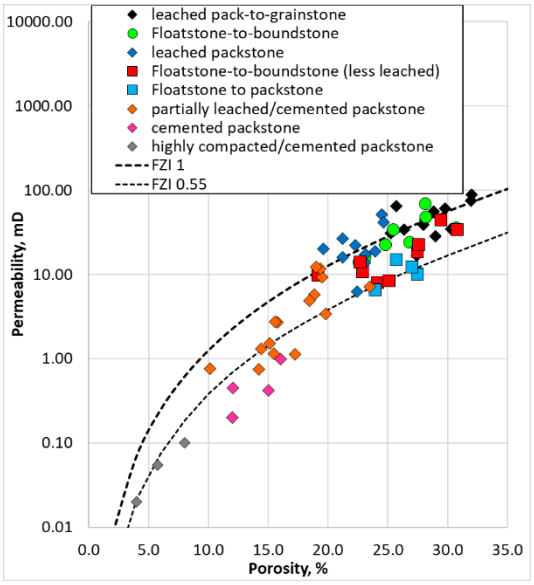

Fig. 14. Highlighted Mixed-texture RRT's with 2 different FZI values. Leached texture RRT's give FZI of 1 with porosity higher than 20%. Less leached textures give FZI 0.55 with the same porosity range. Cemented/compacted textures give FZI 0.55 with porosity less than 20%.

(a) Mixed-texture samples with FZI 1.0 (high porosity)

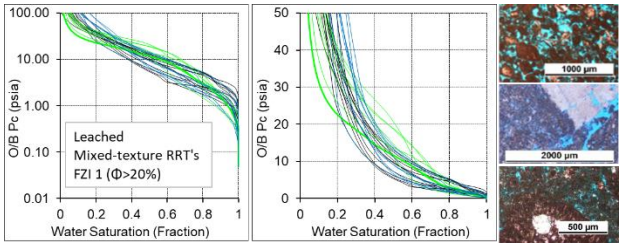

(b) Mixed-texture samples with FZI 0.55 (high porosity)

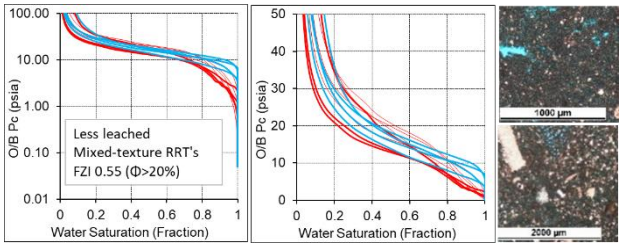

(c) Mixed-texture samples with FZI 0.55 (low porosity)

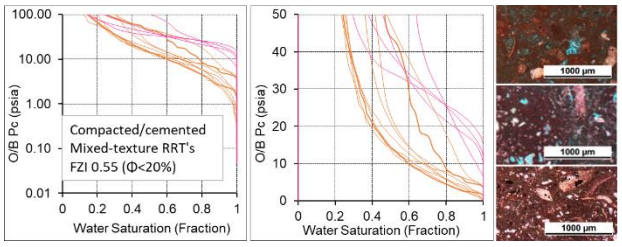

Fig. 15. Mixed RRT samples (from figure 14) grouped by FZI. Semi-log and linear scale Pc plots (along with corresponding TS photomicrographs). (a) Packstone-to-grainstone, floatstone-to-boundstone and leached packstone show similar RRT characteristics and FZI 1.0. (b) Less leached floatstone-to-boundstone and floatstone-to-packstone show similar RRT characteristics and FZI 0.55. (c) cemented/compacted packstone show different RRT's characteristics with similar FZI 0.55. (b) & (c) RRT's are very different and yet have similar FZI 0.55.

Moreover, samples in figure 15(b) and 15(c) do not give similar RRT characteristics although the samples have the same FZI of 0.55. Those RRT's could then be differentiated with a porosity cut-off around 20% based on the detailed Dunham classification as demonstrated in figure 14. For the muddy RRT's, figure 16 groups all the data with 3 different FZI values. The leached wackstone and the leached mudstone samples have FZI values of 0.45 and 0.35, respectively. The recrystallized, compacted and cemented wackstone and mudstone samples all have FZI of 0.25 (porosity < 17%). Figure 17 shows consistency in the Pc and FZI for the leached wackstone and mudstone RRT's. However, the tighter RRT's have shown different Pc behaviour with similar FZI of 0.25.

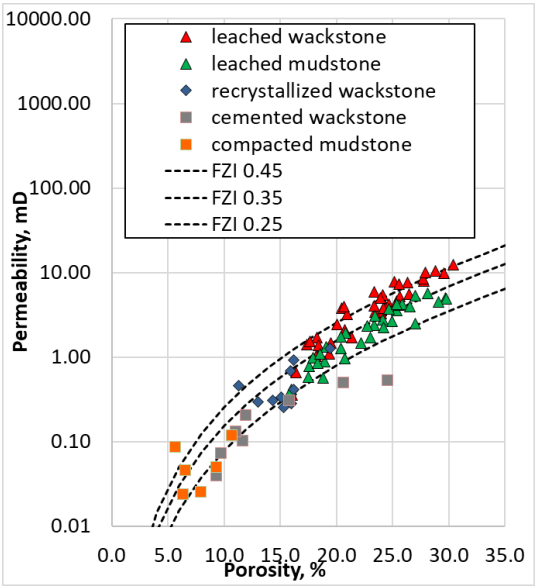

Fig. 16. Highlighted muddy RRT's with 3 different FZI values. Leached wackstone FZI 0.45. Leached mudstone FZI 0.35. Recrystallized/compacted/cemented wackstone and mudstone samples FZI 0.25 (porosity < 17%).

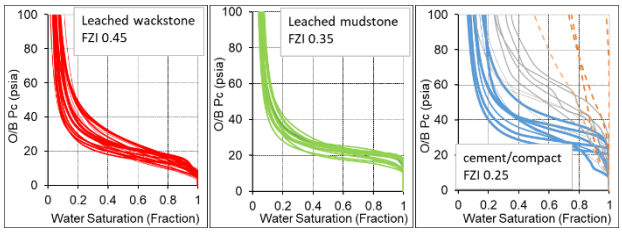

Fig. 17. Muddy RRT samples grouped by FZI.

5.2 Lucia Equation

This empirical method handles permeability in carbonates on the basis of rock-fabric classification, where the flow is related to interparticle porosity [17]. The classification is based on the so called Rock Fabric Number (RFN) that is empirically derived from porosity-water saturation relationships in a number of carbonate samples. Equation (4) and (5) give the empirical calculations of RFN (unitless) and permeability (mD), respectively,

$$\log RFN = \frac{(3.1107+1.8834\log\Phi_g+\log Swi)}{(3.0634+1.4045\log\Phi_g)} \quad (4)$$

$$\log k = 9.7982 - 12.0838 \log RFN + (8.6711 - 8.2965 \log RFN) \log \Phi_g \quad (5)$$

Where
Φ_g is the inter-grain porosity (frac)
Swi is the initial (connate) water saturation (frac)

Equation (4) is constructed on the basis that Swi decreases with porosity for every rock fabric class. Each RFN would have a unique porosity-Sw trend such that RFN increases with Swi for a given porosity. Equation (5) is designed such that permeability decreases with higher RFN for a given porosity. This would then indicate that RFN is expected to increase as we move from the grainy-texture RRT's to the muddy RRT's. In this perspective, an increase in RFN indicates an increase in surface area, hence RFN would be viewed as directly proportional to tortuosity and surface area (opposite to FZI as explained earlier). Nevertheless, the main issue with this method is the fact that it relies on a measure of inter-grain porosity excluding secondary porosity such as vuggy and moldic porosity, which is abundant in carbonate reservoirs. Figure 18 plots log-log scale permeability versus porosity for all the poro-perm data (from figure 1) with Lucia trends constructed from equation (5). Grainy samples show an average RFN 1.7, Mixed 2.85 and Muddy 3.65. Figure 19 gives the semi-log scale plot of figure 18. Because of the difficulty to quantify the interparticle porosity, the plots are given with the total porosity. As with the Kozeny-Carmen model, Lucia shows good overall match to the experimental data except the grainy texture RRT's. This is clearly caused by the high degree of heterogeneity of the grain-size and pore-size systems found in grain-dominated carbonates. The mud in the system seems to produce more unique porosity-permeability relationship, which has been well captured by both investigated models so far (*i.e.* eq. (3) & eq. (5)). Figure 20 depicts the different grainy RRT's in the poro-perm plot. The data can be fitted with 3 different RFN.

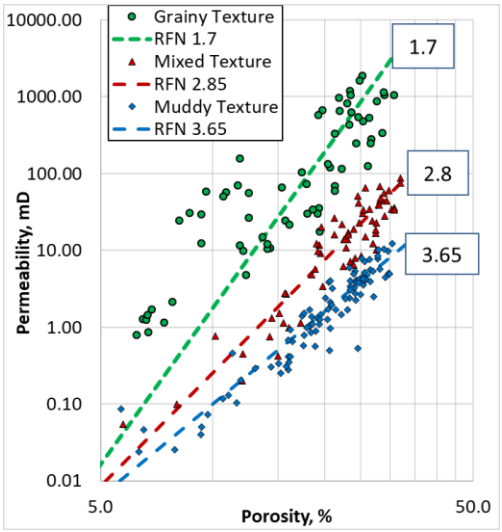

Fig. 18. Log-log scale permeability versus porosity for all the poro-perm data (from figure 1) with Lucia trends plotted from equation (5).

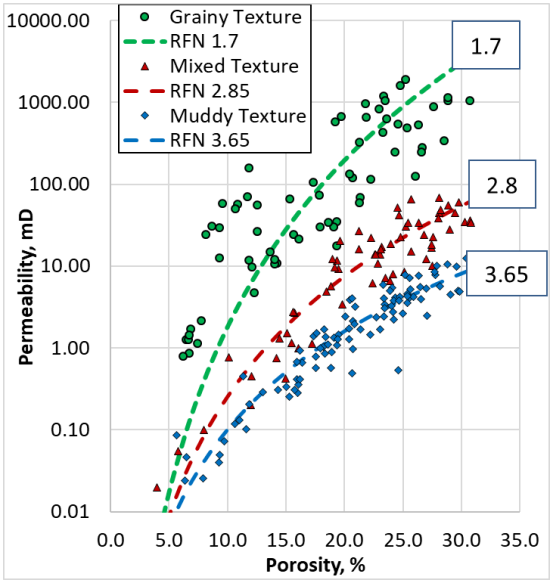

Fig. 19. Semi-log scale of figure 18.

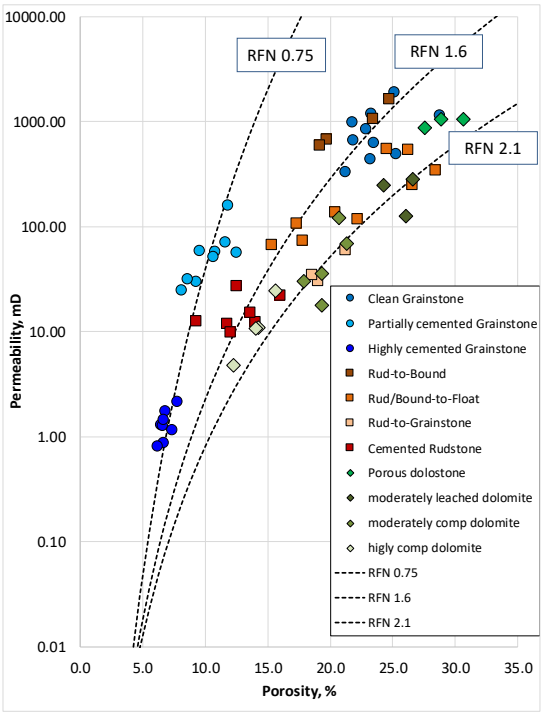

Fig. 20. Highlighted grainy RRT's with 3 different RFN values. Both partially & highly cemented grainstone RRT's gave RFN 0.75. Clean grainstone, Rud-to-Boundstone, low-porosity rud/bound-to-floatstone and cemented rudstone all gave RFN around 1.6. Dolomite with high-porosity Rud/Bound-to-floatstone and rud-to-grainstone gave RFN 2.1. This is a different classification to FZI from figure 12. RFN is not unique per RRT either.

The grouping seem to be different from FZI. RFN 1.6 grouped the clean grainstone RRT together with Rud-to-Boundstone, low porosity Rud/Bound to floatstone and cemented rudstone. The moderately and highly cemented grainstone RRT's were grouped together with a low RFN 0.75. RFN of 2.1 grouped the rest of the RRT's (*i.e.* all the dolomite RRT's together with the high porosity Rud/Bound-to-floatstone and the rud-to-grainstone). These rock types are very heterogeneous with diversified diagenesis processes that produce large grain and pore

size variations, which may not be captured in a single model. Figure 21 shows the mixed-texture RRT's with 2 different RFN. The leached texture RRT's (i.e. packstone-to-grainstone, floatstone-to-boundstone and packstone) give RFN of 2.7. The less leached textures give RFN 3.2. This is almost a similar behaviour to the FZI model. For the muddy RRT's, figure 22 groups all the data with 2 different RFN only. The leached wackstone and the leached mudstone samples have RFN values of 3.45 and 3.75, respectively. The low porosity recrystallized, compacted and cemented wackstone and mudstone samples all have similar RFN of 3.75.

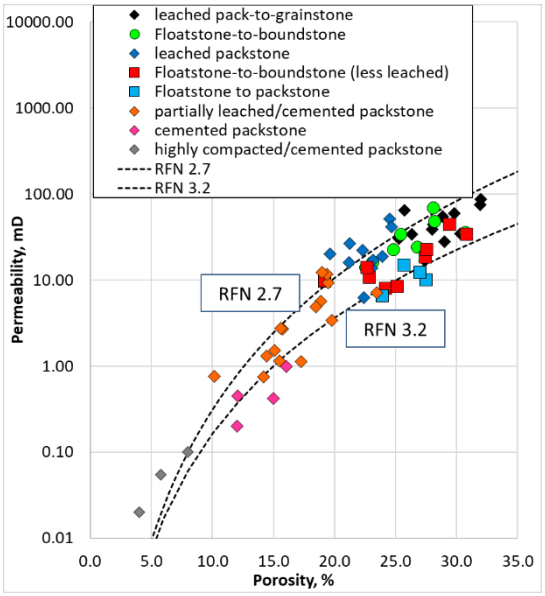

Fig. 21. Highlighted Mixed-texture RRT's with 2 different RFN values. Leached texture RRT's give RFN 2.7 with porosity higher than 20%. Less leached textures give RFN 3.2 with the same porosity range. Cemented/compacted textures give RFN 3.2 with porosity less than 20%.

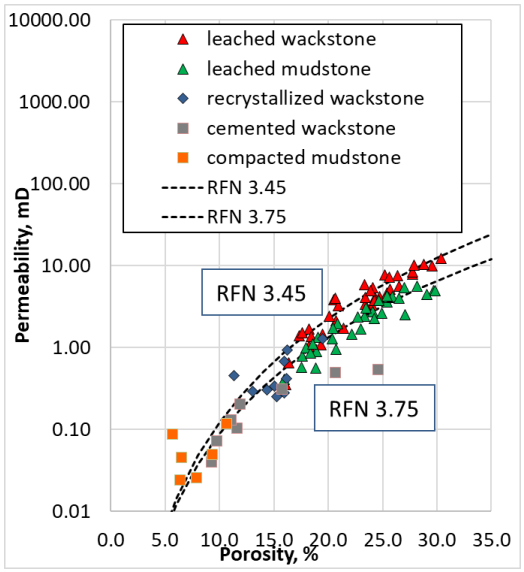

Fig. 22. Highlighted muddy RRT's with 2 different RFN values. Leached wackstone RFN 3.45. Leached mudstone RFN 3.75. Recrystallized/compacted/cemented wackstone and mudstone samples RFN 3.75 (porosity < 17%).

5.3 Winland Equation

Dale Winland of Amoco [18] used mercury injection-capillary pressure curves to develop an empirical relationship between porosity, permeability and pore throat radius (r). He tested sandstone and carbonate samples, and found that the effective pore system that dominates flow through a rock corresponds to a mercury saturation of 35%. He named that pore system r35. That pore system has pore throat radii equal to the pore throats entered when a rock is saturated 35% with a non-wetting phase. After 35% of the pore system fills with a non-wetting phase fluid, the remaining pore system does not contribute to flow. Instead, it contributes to storage. Winland never published his equation, rather it was later published by Kolodzie as in equation (6) below,

$$\text{Log}(r35) = 0.732 + 0.588\log k - 0.864\log\Phi \qquad (6)$$

Where
r35 is the pore throat radius at 35% mercury saturation (micron)
Φ is the porosity (%)
k is the uncorrected air permeability (mD)

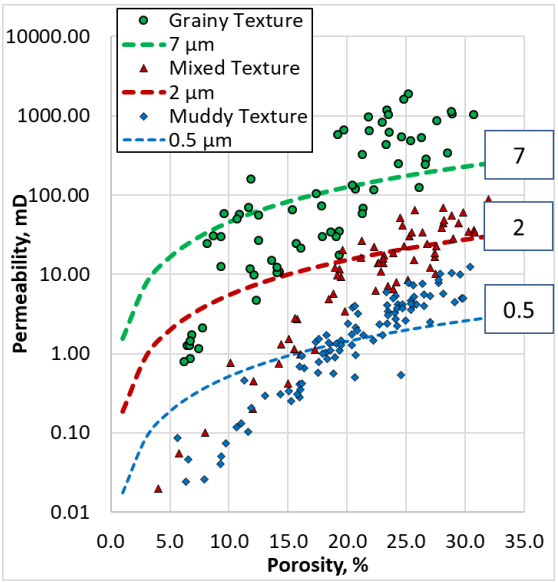

Fig. 23. Permeability versus porosity for all the poro-perm data (from figure 1) with r35 trends plotted from equation (6). The Winland trends have very different slopes compared to the texture-based experimental behaviour.

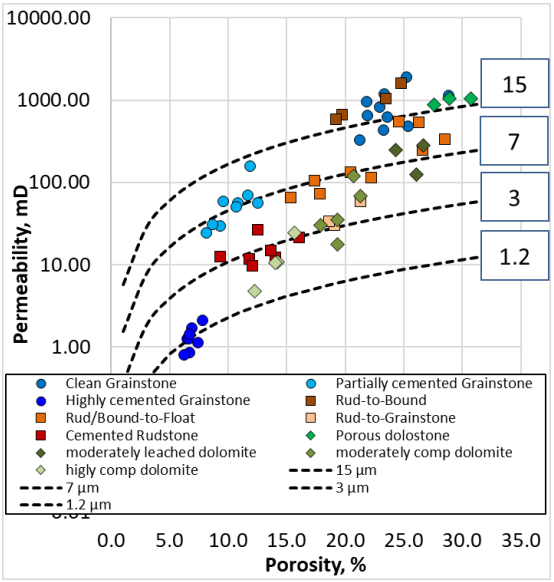

Fig. 24. Highlighted grainy RRT's with 4 different r35 micron values. Porous dolostone, clean grainstone, rud-to-boundstone and high porosity rud/bound-to-floatstone gave simailr r35 of 15 microns. Moderately leached dolomite with low porosity rud/bound-to-floatstone and the moderately cemented grainstone all gave r35 of 7 micron. Cemented/compacted dolomite together with cemented rudstone and rud-to-grainstone gave r35 of 3 microns. The highly cemented grainstone showed the least r35 at 1.2 microns.

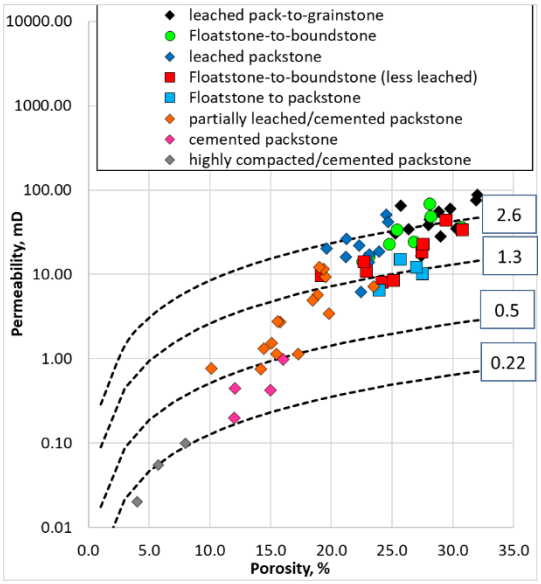

Fig. 25. Highlighted Mixed-texture RRT's with 4 different r35 micron values.

It is claimed that this method provides a more scientific approach for rock quality characterisation than simply using the porosity-permeability distribution. It was used to identify flow units in the reservoir by computing r35 from porosity and permeability, where the flow units are grouped by the size of the pore throats [19]. To evaluate this method, figure 23 gives the permeability versus porosity for all the poro-perm data (from figure 1) with Winland r35 trends constructed from equation (6).

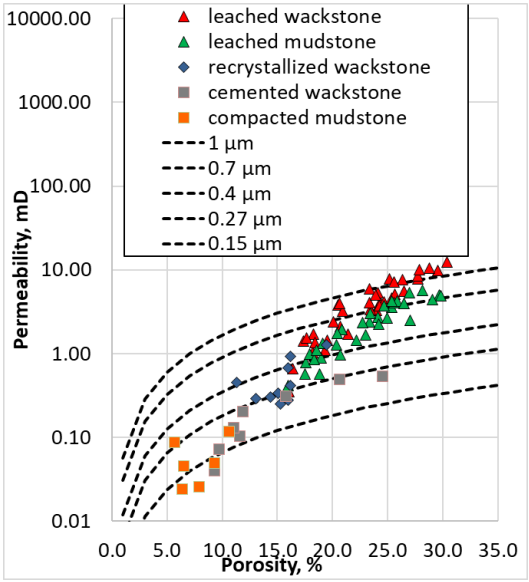

Fig. 26. Highlighted muddy RRT's with 5 different r35 values.

Grainy samples show an average r35 of 7 microns, Mixed 2 microns and Muddy 0.5 microns. The Winland trends have very different slopes compared to the texture-based experimental behaviour with minimal coverage of the texture trends. It is clear that r35 analysis has no strong link to the geology of the rock types. The previous approaches (FZI & RFN) seem to better honour the geology of the samples within the porosity-permeability domain. Figure 24 highlights the grainy RRT's with 4 different r35 micron values. Porous dolostone, clean grainstone, rud-to-boundstone and high porosity rud/bound-to-floatstone gave similar r35 of 15 microns. Moderately leached dolomite with low porosity rud/bound-to-floatstone and the moderately cemented grainstone all gave r35 of 7 micron. Cemented/compacted dolomite together with cemented rudstone and rud-to-grainstone gave r35 of 3 microns. The highly cemented grainstone showed the least r35 at 1.2 microns. These fitting r35 values do not necessarily reflect the true r35 of the samples and the permeability predictions based on equation (6) vary within +/- factor of 5. This method gives a very different classification to FZI and RFN from figure 12 and figure 21, respectively. R35, again, does not provide unique flow units (RRT's) in the reservoir. Figure 25 highlighted the mixed-texture RRT's with 4 different r35 micron values. Leached texture RRT's (with porosity higher than 18%) gave average micron range 2.6 to 1.3 microns, while less leached textures (with lower porosity range) gave r35 values between 0.5 and 0.22 microns. Figure 26 highlights the muddy RRT's with 5 different r35 values. Leached wackstone and mudstone RRT's gave r35 range between 1 and 0.4 microns. Recrystallized/compacted/cemented wackstone and mudstone samples show average range of r35 between 0.27 and 0.15 microns. While the porosity-permeability relationship can be described by one or two trends using FZI or RFN, Winland models the permeability with 5 trends based on varying pore sizes in the muddy RRT's.

6 Summary and Conclusions

Representative carbonate samples were selected from 7 reservoirs across the Middle East Region. Unique rock types were established based on porosity-permeability characteristics, capillary pressure and textural facies. Three main porosity-permeability trends were identified based on textures. Carmen-Kozeny (FZI), Lucia (RFN) and Winland (r35) permeability equations were used to model the experimental data. The following conclusions can be derived from this study,

1. Three porosity-permeability correlations were derived for the 3 main textures by (best-fit) power regression. The power equations can predict permeability with uncertainty factor of +/- 2 (figure 1).
2. Grainy RRT's showed the highest degree of permeability variation within the same porosity range. Muddy samples can be satisfactorily described by a single power correlation.
3. Three FZI trends modelled the porosity-permeability data and honoured the geological textures (figure 11). Permeability can be estimated with a factor of +/- 2 but the samples with the same FZI do not necessarily represent similar flow unit as originally claimed.
4. Three RFN trends modelled the porosity-permeability data and honoured the geological textures (figure 19). For the grainy RRT's, permeability estimation can vary +/- one order of magnitude (a factor of 10) but the prediction is much better for the mixed and muddy RRT's (factor of +/- 2). Samples with same RFN do not necessarily represent similar flow unit.
5. Winland r35 trends poorly modelled the experimental data (figure 23) and did not conform to the texture-based correlations.

The authors wish to acknowledge the support from Abu Dhabi National Oil Company (ADNOC) and Ingrain - Halliburton.

References

1. S.K. Masalmeh and X.D. Jing, The Importance of Special Core Analysis in Modelling Remaining Oil Saturation in Carbonate Fields, SCA2008-03 (2008)
2. M. Dernaika, Z. Kalam, S. Skjaeveland, Understanding Imbibition Data in Complex Carbonate Rock Types, SCA2014-59 (2014)
3. J.J.M. Buiting, E.A. Clerke, Permeability from porosimetry measurements: Derivation for a tortuous and fractal tubular bundle, J Petrol Sci Eng, (2013) http://dx.doi.org/10.1016/j.petrol.2013.04.016i
4. M.R. Dernaika, Y. Naseer Uddin, S. Koronfol, O. Al Jallad, G. Sinclair, Multi-Scale Rock Analysis for Improved Characterization of Complex Carbonates, SCA2015-034 (2015)
5. M.R. Dernaika, B. Mansour, D. Gonzalez, S. Koronfol, F. Mahgoub, O. AlJallad, M. Contreras, Upscaled Permeability and Rock Types in a Heterogeneous Carbonate Core from the Middle East, SPE-185991-MS (2017)
6. M.R. Dernaika, and G.G. Sinclair, Resolving the Link between Porosity and Permeability in Carbonate Pore Systems, SCA2017-77 (2017)
7. M. Mousavi, M. Prodanovic, and D. Jacobi, New Classification of Carbonate Rocks for Process-Based Pore-Scale Modeling, SPE 163073, SPE J. (2013)
8. R.J. Dunham, Classification of Carbonate Rocks According to Depositional Texture. In Classification of Carbonate Rocks: A Symposium. American Association of Petroleum Geologists Memoir 1, ed. W.E. Ham, 108-121. Tulsa, Oklahoma: AAPG (1962)
9. H. Al-Owihan, M. Al-Wadi, S. Thakur, S. Behbehani, N. Al-Jabari, M. Dernaika, and S. Koronfol, Advanced Rock Characterization by Dual-Energy CT Imaging: A Novel Method for Complex Reservoir Evaluation, IPTC 17625 (2014)
10. M.R. Dernaika, B. Mansour, O. AlJallad, Characteristics of Carbonate Rock Types in the Middle East, SCA2018-65 (2018)
11. S. Serag El Din, M.R. Dernaika, M.Z. Kalam, and L. Hannon, The Effect of Rock Properties on Residual Oil Saturation in Heterogeneous Carbonate Rocks, SPE-164141 (2013)
12. S.K. Masalmeh and X.D. Jing, Improved Characterization and Modelling of Carbonate Reservoirs for Predicting Waterflood Performance, IPTC-11722-MS (2007)
13. J.O. Amaefule, M. Altunbay, D. Tiab, D.G. Kersey, and D.K. Keelan, Enhanced Reservoir Description: Using Core and Log Data to Identify Hydraulic (Flow) Units and Predict Permeability in Uncored Intervals/Wells, SPE 26436 (1993)
14. A.K. Ambastha, and T.J. Moynihan, A Simple And Accurate Method For An Integrated Analysis Of Core And Log Data To Describe Reservoir Heterogeneity, Petroleum Society of Canada. doi:10.2118/96-01-06 (1996)
15. J. Kozeny, Uber Kapillare Leitung des Wassel'S im Boden, Sitzungsberichte, Royal Academy of Science, Vienna, Proc. Class I **136**, 271-306 (1927)
16. P.E. Carmen, Fluid Flow through Granular Beds, Trans. AIChE **15**, 150 -166 (1937)
17. J.W. Jennings, and F.J. Lucia, Predicting Permeability From Well Logs in Carbonates With a Link to Geology for Interwell Permeability Mapping, SPE-84942 (2003)
18. S. Kolodzie, Analysis of Pore Throat Size And Use of the Waxman-Smits Equation To Determine OOIP in Spindle Field, Colorado, SPE 9382 (1980)
19. A.J. Martin, S.T. Solomon, and D.J. Hartmann, Characterization of Petrophysical Flow Units in Five Carbonate Reservoirs. American Association of Petroleum Geologists Bull. 81 (5):734 (1997).